

Metal-Decorated InN Monolayer Senses N₂ against CO₂

Lin Tao,^{*,∇} Davoud Dastan,^{*,∇} Wensen Wang, Preeyaporn Poldorn, Xianze Meng, Mingjie Wu, Hongwei Zhao, Han Zhang, Lixiang Li,^{*} and Baigang An^{*}

Cite This: *ACS Appl. Mater. Interfaces* 2023, 15, 12534–12544

Read Online

ACCESS |

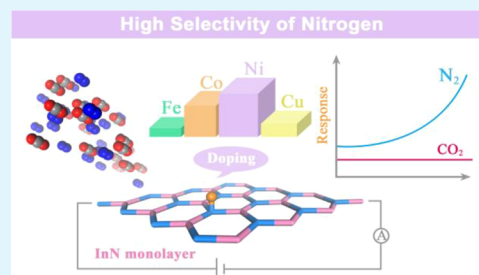
Metrics & More

Article Recommendations

Supporting Information

ABSTRACT: Poor selectivity is a common problem faced by gas sensors. In particular, the contribution of each gas cannot be reasonably distributed when a binary mixture gas is co-adsorbed. In this paper, taking CO₂ and N₂ as an example, density functional theory is used to reveal the mechanism of selective adsorption of a transition metal (Fe, Co, Ni, and Cu)-decorated InN monolayer. The results show that Ni decoration can improve the conductivity of the InN monolayer while at the same time demonstrating an unexpected affinity for binding N₂ instead of CO₂. Compared with the pristine InN monolayer, the adsorption energies of N₂ and CO₂ on the Ni-decorated InN are dramatically increased from -0.1 to -1.93 eV and from -0.2 to -0.66 eV, respectively. Interestingly, for the first time, the density of states demonstrates that the Ni-decorated InN monolayer achieves a single electrical response to N₂, eliminating the interference of CO₂. Furthermore, the d-band center theory explains the advantage of Ni decorated in gas adsorption over Fe, Co, and Cu atoms. We also highlight the necessity of thermodynamic calculations in evaluating practical applications. Our theoretical results provide new insights and opportunities for exploring N₂-sensitive materials with high selectivity.

KEYWORDS: InN monolayer, N₂ sensing, electrical response, transition metal decorated, density functional theory



1. INTRODUCTION

In contrast to conventional metal oxide semiconductors,^{1,2} two-dimensional (2D) materials³ have drawn tremendous attention owing to their high specific surface area and high electrical response to gas environments, which are the key characteristics for applications in chemical sensing.^{4–12} After discovering graphene and acquiring its extraordinary properties,¹³ 2D group III nitrides¹⁴ also show high thermal stability and exceptional electron mobility, making them an archetypal candidate in gas sensing applications.^{15–21} In addition, Mortazavi et al.^{22,23} used machine learning interatomic potentials to demonstrate that two-dimensional materials have excellent mechanical properties.

Previous studies have shown that the chemical environment of nitrogen atoms on the surface of group III nitrides is more favorable for CO₂ adsorption,²⁴ which can be attributed to the electrostatic interaction between the O atom in CO₂ and the N atom in the adsorbent.²⁵ Thus, it has a clear affinity for the selective adsorption of CO₂ over N₂. For instance, the strong adsorption of CO₂ on the AlN monolayer has a potential for application in carbon capture and storage, compared with the computed adsorption features of N₂.^{24,26} In addition, *h*-BN nanosheets also show preferential adsorption features of CO₂ due to their greater adsorption energy of CO₂ than N₂.^{16,17,27} By comparison, the InN monolayer exhibits a more selective adsorption capacity of CO₂ over N₂, which indicates that N₂ possesses weak interaction with the metal nitrides.²⁶ However, the selective adsorption of pure metal nitrides mentioned above is achieved based on weak interactions.

It is well known that the mechanism of gas sensing involves the electron transfer or co-existence (electrical response) between gas molecules and adsorbents.^{28–30} Weak interactions do not induce a significant electrical response.^{31–34} Transition metal (TM) decoration as a cost-effective and facile method can effectively enhance their electric conductivity³⁵ and electrochemical performance due to the strong interactions between gas molecules and adsorbents.^{36–41} Among them, the InN monolayer is considered an excellent candidate for decorating. Guo et al.⁴² reported that noble metal atom (Pd, Pt, Ag, and Au)-decorated InN monolayers as a gas sensing material could cause an obvious electrical response of NO₂ adsorption.

Moreover, Cui et al.⁴³ found that Ni-decorated InN monolayers can be employed as resistive sensors for detecting NO, CO₂, and NH₃, which is attributed to the trend of electrical response changes. For the detection of hazardous gas in the electric industry, Chen et al.⁴⁴ certified that Cu-decorated InN monolayers remarkably improved the chemical interplays with SF₆ decomposition products according to the electronic features of all adsorption principles. Furthermore,

Received: November 29, 2022

Accepted: February 2, 2023

Published: February 22, 2023



since H_2 is a flammable and explosive gas,^{29,30} Rh- and Cu-decorated InN monolayers have been proven effective in hydrogen adsorption and sensitive materials.^{45,46} In summary, gas sensing in the above-mentioned studies is based on the density of states (DOS) of TM-decorated InN (TM-InN) monolayers, which obtain the change in electrical response caused by gas adsorption. This is because the electrical response is positively related to the height of DOS at the Fermi level.^{47–50}

It is worth noting that the value of the electrical response is used to judge the gas sensing of the TM-InN monolayer in the above-mentioned studies. However, when a mixture of gases is co-adsorbed, their electrical responses show the same trend, either enhanced or weakened. Meanwhile, the electrical response of the TM-InN monolayer is derived from the sum of the contributions of each gas. The critical scientific problem is that there is no effective way to rationally distribute each gas's contribution. Therefore, when two gases are co-adsorbed, the way to improve selectivity is to eliminate the electrical response of one of them.^{19–21} Taking the chemical inert gases CO_2 and N_2 as an example, if the activation of N_2 chemical bonds or the elimination of the electrical response to CO_2 is broken through, the N_2 sensor will have great significance for monitoring the process of gas separation, synthesis, and nitrogen reduction reaction (NRR).^{51–60}

In this study, density functional theory (DFT) with dispersion-corrections was used to investigate the gas selectivity of CO_2 and N_2 on the TM-InN monolayer. At first, the stability of TM (Fe, Co, Ni, and Cu)-decorated InN monolayers was determined by calculating their binding energy. Then, the adsorption behaviors of CO_2 and N_2 on TM-InN monolayers were systematically discussed compared with the pristine InN monolayer according to the gas–solid interface interaction parameters. Notably, the Ni-decorated InN monolayer achieves a single electrical response to N_2 which is characterized by the accompanied DOS analysis. In addition, the d-band center theory was used to reveal the underlying mechanism of advantages of Ni atom decorating. Finally, the practical application environment of the TM-InN monolayer as a N_2 sensor is evaluated by thermodynamic calculations. Our theoretical research provides new insights into the design of highly selective gas sensors.

2. METHODS

For the pristine InN monolayer, TM-InN monolayer, CO_2 , and N_2 , all of the calculations on structure optimization and electronic properties were performed using DFT, based on Dmol³ code.⁶¹ Under the Perdew–Burke–Ernzerhof functional, the method of the generalized gradient approximation was utilized to define the exchange–correlation interaction.^{62,63} The double numerical basis set with polarization function was used to deal with the atomic orbital. A dispersion-corrected DFT (DFT-D) method was selected based on the Grimme vdW correction,⁶⁴ which can accurately describe weak interactions in all calculations. The radius of real-space global cutoff was 4.9 Å, and the Brillouin zone was sampled by $3 \times 2 \times 1$ k-points utilizing the Monkhorst–Pack scheme to accomplish high-quality theoretical evaluations. Moreover, the convergence tolerances of geometry optimizations were 1×10^{-5} Ha for the total energy, 0.002 Ha/Å for atomic forces, and 0.005 Å for the highest displacement, respectively. The electron distribution and charge transfer were calculated by the Mulliken method.⁶⁵ The InN crystal structure was optimized to construct the pristine InN monolayer. The lattice parameter of the InN crystal is 3.55 Å, which agrees with the previous reports.^{26,66,67} To eliminate the interaction between periodic images, a 20 Å vacuum layer was used vertically to the InN monolayer.

3. RESULTS AND DISCUSSION

3.1. Pristine InN Monolayer. In this section, the accuracy of the pristine structure of the InN monolayer was initially confirmed. Then, the gas adsorption properties on the as-prepared InN monolayer were thoroughly evaluated. Since there are few related studies, discussing the gas adsorption behavior of the pristine InN monolayer is necessary. Figure 1

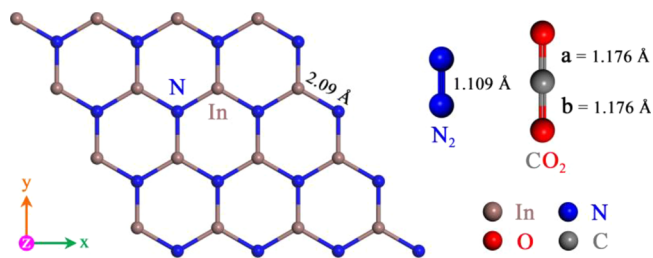


Figure 1. Pristine InN monolayer, N_2 , and CO_2 structures and parameters.

shows the as-prepared InN monolayer with an optimal bond length of 2.09 Å between In and N. This result is consistent with previous studies. In addition, the optimized bond lengths of CO_2 and N_2 molecules are also uniform with reports in the literature.^{56–58}

Figures S1 and S2 show that the horizontal and vertical adsorption configurations of CO_2 and N_2 are established at two adsorption sites (In and N) of the InN surface, according to previous studies.²⁶ Then, the charge density distribution is calculated based on the most stable adsorption configurations. The results show that CO_2 and N_2 all maintain weak physisorption for whatever the adsorption configuration, which can be attributed to the noncontact electron cloud between gas molecules and the adsorption site. Further, the adsorption energy and adsorption distance of CO_2 and N_2 are calculated precisely. The results are displayed in Figure S3, where it can be seen that the adsorption energy of CO_2 is more negative than N_2 . Hence, CO_2 has the shortest adsorption distance. Significantly, the results confirm that the selective adsorption of CO_2 and N_2 by the pure InN monolayer is due to weak interactions and will not cause an electrical response.

3.2. TM-InN Monolayer. To study the eventual electrical response of the TM-InN membrane to CO_2 and N_2 , we first constructed the InN monolayer decorated with four TM atoms (Fe, Co, Ni, and Cu). Then, the stability of the decorating structure is assessed by both the binding energy and the cohesive energy. Finally, the effect of TM decoration on structural conductivity is evaluated by DOS analysis.

Figure 2 shows the stable TM-InN structures and the calculated charge density distribution. The results show that the TM-InN monolayer structure is not significantly altered after TM decoration, implying that the TM-InN system is stable. Not only that, from the charge density, it is found that the electronic wavefunction of the TM atoms overlaps significantly with the electronic states of the InN monolayer, displaying the charge accumulation of TM atoms and the charge depletion of the InN monolayer. In addition, the N atoms show the charge accumulation against the In atoms. An apparent decrease in the charge accumulation occurs on the nearest N atom of the TM atoms. These results suggest that the TM atoms can be anchored on the InN monolayer.

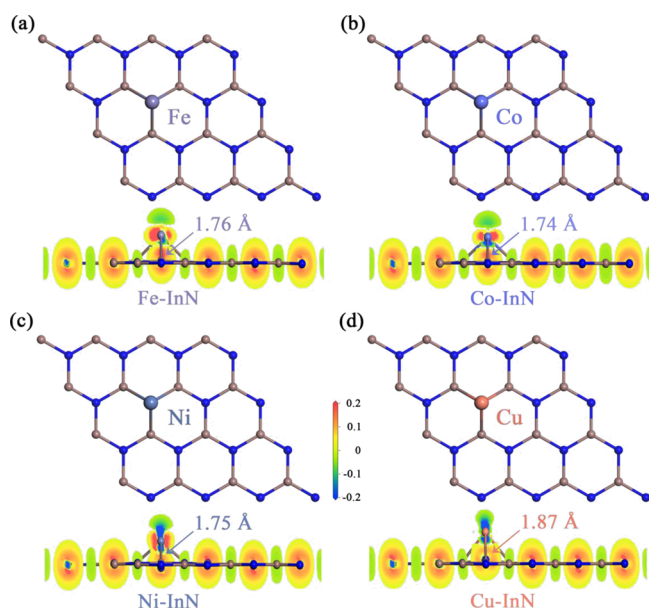


Figure 2. Stable structures and electron density distribution of TM-InN (a) Fe-InN, (b) Co-InN, (c) Ni-InN, and (d) Cu-InN. Densities are displayed with an isosurface and the interval of isovalue is between -0.2 and 0.2 $e/\text{\AA}^3$.

To confirm that the TM atoms bind strongly to the InN monolayer, rather than undergo aggregation,⁴³ the binding energy (E_b) is used to quantitatively describe the stability of TM-InN, defined as

$$E_b = E_{\text{TM-InN}} - E_{\text{InN}} - E_{\text{TM}} \quad (1)$$

where $E_{\text{TM-InN}}$ is the energy (eV) of TM-InN, E_{InN} is the energy (eV) of the pure InN monolayer, E_{TM} is the energy (eV) of TM. Figure S4a shows the minimum binding energy guaranteed for the chemisorption (about -0.52 eV⁵⁹). The calculation results prove that the binding energy of the TM atoms to the InN monolayer is much larger than the minimum of chemisorption. It strongly suggests that the four TM atoms form strong bonds to the InN monolayer and would not aggregate. Moreover, the stability of the TM-InN monolayer is another essential indicator and is usually expressed by cohesive energy (E_{coh}), defined as

$$E_{\text{coh}} = \frac{(n_1 E_{\text{TM}} + n_2 E_{\text{In}} + n_3 E_{\text{N}} - E_{\text{InN}})}{(n_1 + n_2 + n_3)} \quad (2)$$

where E_{In} and E_{N} represent the energies (eV) of In and N atoms, respectively; n_1 , n_2 , and n_3 are the numbers of TM, In, and N atoms. In Figure S4b, the cohesive energy of the pristine InN monolayer is -3.46 eV/atom. In contrast, the effect of TM decoration on the InN monolayer stability is almost

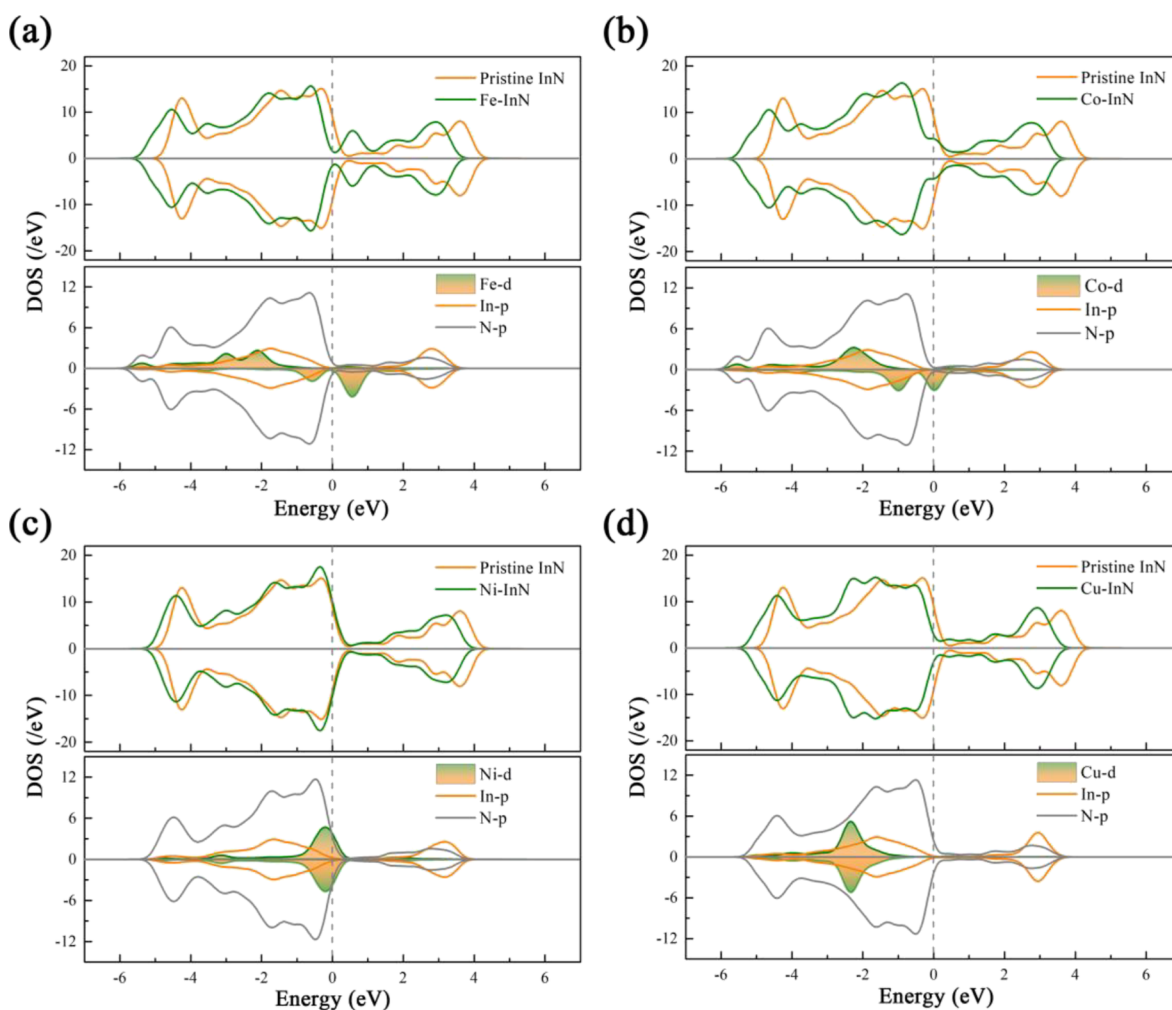


Figure 3. DOS of (a) Fe-InN, (b) Co-InN, (c) Ni-InN, and (d) Cu-InN. Fermi energy was set zero indicated by the vertical dashed line.

negligible. In addition, Figure S5 shows that the TM-InN monolayers are thermodynamically stable based on the results of the ab initio molecular dynamics simulation (AIMD). Therefore, the above results prove that the TM-InN monolayers are stable.

Excellent electron conduction capability is an essential indicator of gas sensors. It is necessary to analyze the DOS of the TM-InN monolayer because the DOS can be used to describe the electrical conductivity of materials.^{49,50} Figure 3 shows the DOS of the pristine and TM-decorated InN monolayer. For the Fe-InN, Co-InN, and Cu-InN systems, the heights of their total DOS are lower than that of pristine InN at the Fermi level. It suggests that Fe, Co, and Cu decoration reduces the surface conductivity of InN. On the contrary, decorating Ni atom causes a slight increase in the conductivity of InN. Further, there is a significant overlap between the TM atoms' d orbitals and the N atom's p orbital, confirming strong hybridization. Therefore, these results demonstrate that decorating Ni atom is more beneficial in improving the surface conductivity of the InN monolayer.

3.3. Gas Sensing Behavior on the TM-InN Monolayer.

3.3.1. Gas Adsorption Behavior. In this part, we first confirm the most stable adsorption configuration of CO₂ and N₂ on the TM-InN monolayer. Then, the electron density distribution of the optimal adsorption configuration is calculated. Lastly, the adsorption nature of CO₂ and N₂ on the TM-InN monolayer was thoroughly investigated based on adsorption energy, adsorption distance, charge transfer, bond length, and bond order of gas.

As shown in Figure S6, CO₂ horizontally adsorbed on the TM atom sites is constructed. It can be found that there is a weak adsorption between CO₂ and the TM-InN monolayer, which is attributed to no significant charge accumulation or depletion. In contrast, Figure 4 shows a more stable vertical adsorption configuration of CO₂. A distinct electronic overlap between CO₂ and TM atoms can represent a stronger charge

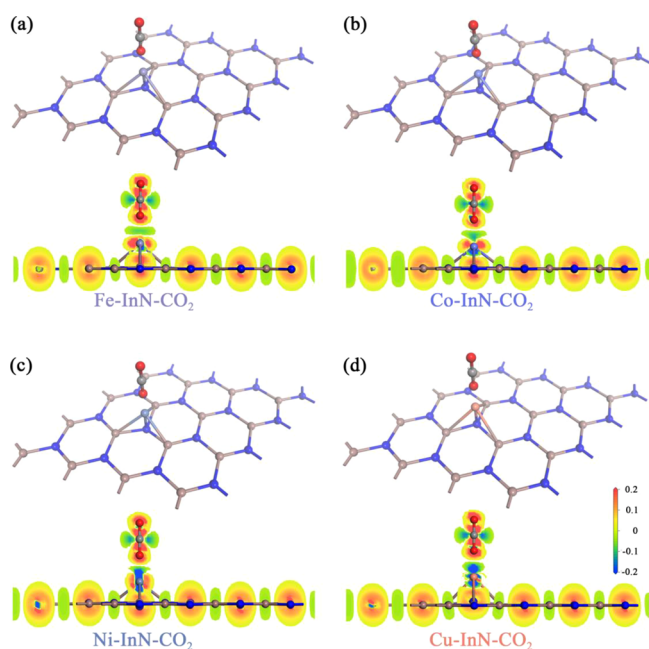


Figure 4. Most stable gas–solid adsorption interface and electron density distribution. (a) Fe-InN-CO₂, (b) Co-InN-CO₂, (c) Ni-InN-CO₂, and (d) Cu-InN-CO₂.

accumulation and depletion than horizontal configurations. Therefore, CO₂ prefers the vertical adsorption configuration on the TM-InN monolayer.

Furthermore, Figure S7 shows N₂ horizontally adsorbed on the TM sites. A distinct overlap of electrons can be found between the gas and surface, indicating that the TM-InN has an apparent affinity toward N₂. Notably, N₂ shows a more stable vertical adsorption configuration as shown in Figure 5.

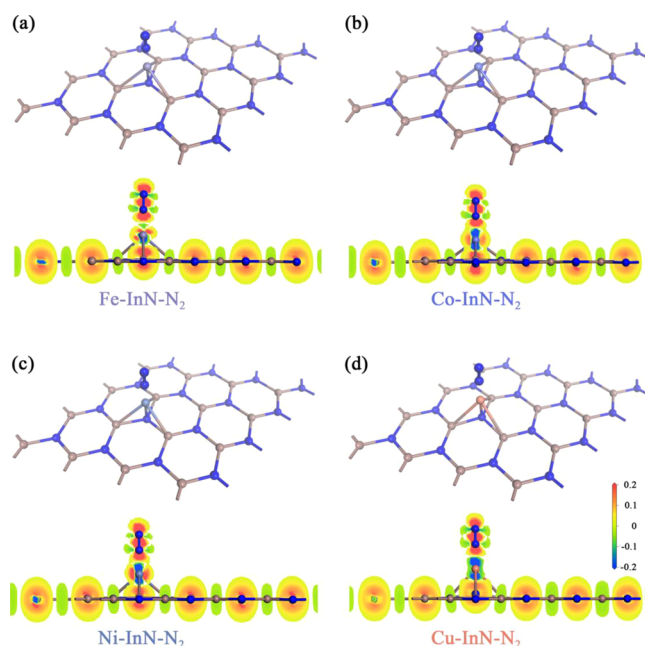


Figure 5. Most stable gas–solid adsorption interface and electron density distribution. (a) Fe-InN-N₂, (b) Co-InN-N₂, (c) Ni-InN-N₂, and (d) Cu-InN-N₂.

Stronger adsorption exists between the vertical N₂ and the TM-InN monolayer, according to the charge density distribution. It indicates that the vertical N₂ is the optimal adsorption configuration.

To accurately compare the adsorption behavior of CO₂ and N₂ mentioned above, adsorption energy and distance are calculated. The adsorption energy (E_{ads}) is defined as

$$E_{\text{ads}} = E_{\text{total}} - (E_{\text{surface}} + E_{\text{gas}}) \quad (3)$$

where E_{total} and E_{gas} are the total energy (eV) of the monolayer and isolated gas molecule, respectively, and E_{surface} is the total energy (eV) of the monolayer surface. Figures S8 and 6a show the results of calculations corresponding to the horizontal and vertical configurations. It can be found that the TM-InN monolayer has a stronger affinity toward N₂ than CO₂, regardless of configurations. Furthermore, both CO₂ and N₂ prefer vertical adsorption, due to shorter adsorption distances and greater adsorption energy. In detail, the order of CO₂ adsorption energy is as follows: Ni-InN > Cu-InN > Co-InN > Fe-InN. The order of N₂ adsorption energy is as follows: Ni-InN > Co-InN > Cu-InN > Fe-InN. In addition, these trends can be proved by crystal orbital Hamilton population (COHP) analysis as shown in Figures S9 and S10. For CO₂ and N₂, Ni-InN and Fe-InN have the highest and the lowest adsorption energy, respectively. However, the adsorption energy of CO₂ on Cu-InN is more negative than that of Co-InN, with the

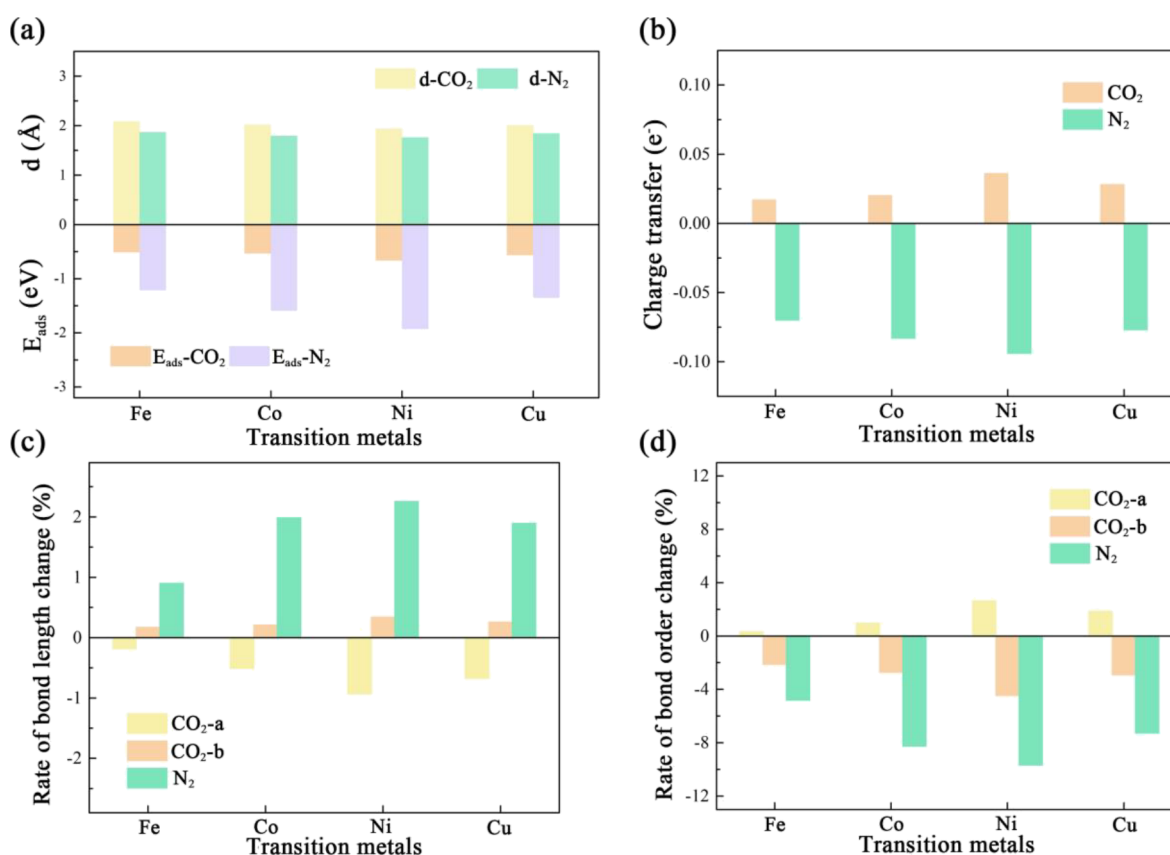


Figure 6. Adsorption properties of CO₂ and N₂ on the TM-InN monolayer. (a) Adsorption energy and adsorption distance, (b) charge transfer, (c) rate of bond length change, and (d) rate of bond order change.

opposite of N₂. It shows that Ni is the best decorated atom due to the optimal adsorption performance.

Moreover, the amount of charge transfer of CO₂ and N₂ on the Ni-InN monolayer is also the largest as shown in Figure 6b. The 0.094 electrons are injected into the N₂, while CO₂ loses the 0.036 electrons on the Ni-InN monolayer. To quantitatively characterize the effect of TM decorating on gas molecules, we calculate their bond length and the Mayer bond order. According to our calculations, the bond lengths of free CO₂ and N₂ are 1.176 and 1.108 Å, respectively. The Mayer bond orders of free CO₂ and N₂ are 1.286 and 1.539, respectively. Since CO₂ has a vertical adsorption configuration, we define two bonds of a and b according to Figure 1. In addition, the rate of bond length and the Mayer bond order change are calculated to make it more intuitive (Figure 6c,d).

One can find that the effect of Ni decoration on CO₂ and N₂ is also the most prominent. Among these, the a-bond of CO₂ is compressed and the b-bond is elongated. It means that the b-bond close to the TM site is activated, enhancing of the a-bond. Importantly, the bond length of N₂ changes dramatically (from 1.108 to 1.133 Å), indicating that the chemically inert triple bond between N atoms is activated. In contrast to the reported superior NRR catalysts, such as the bond length of N₂ on a Janus Fe-SnO₂ is 1.136 Å, that of Fe introduced S-doped carbon is 1.14 Å,⁶⁰ that of Mo-doped borophene is 1.125 Å,⁶⁷ and that of the boron nanosheet is 1.132 Å⁶⁷; the Ni-InN monolayer shows an excellent activation capacity to N₂. Meanwhile, the rate of the Mayer bond order change also proves that N₂ is activated, which causes a considerable decrease in the bond strength of the triple bond in N₂. Thus,

these reasons cause the Ni-InN monolayer to maintain the affinity toward N₂.

3.3.2. Electrical Response Behavior. To clarify the electrical response of TM-InN to CO₂ and N₂ adsorption, DOS is used to describe the changes in electrical conductivity. Figure 7 shows the change in DOS of the TM-InN monolayer after CO₂ adsorption. The higher the height of the DOS curve at the Fermi level, the stronger the conductivity. Except for the Ni-InN, the electrical responses caused by CO₂ adsorption on the surface of Fe-InN, Co-InN, and Cu-InN are reduced (left-shifted). The adsorbed CO₂ contributes substantially to the DOS deformation of TM-InN. At the same time, hybridization appears between the *p* orbital of gas and the *d* orbital of TM atoms, which indicates that CO₂ interacts with the TM-InN monolayer. Importantly, the adsorption of CO₂ does not change the conductivity of the Ni-InN monolayer (height overlap at the Fermi level). This strong evidence suggests that the Ni-InN monolayer can achieve the elimination of electrical response to CO₂.

Figure 8 shows the DOS of the N₂ adsorbed TM-InN monolayer. The surface conductivities of Fe-InN, Co-InN, and Cu-InN are reduced with N₂ adsorption. Interestingly, the surface conductivity of the Ni-InN monolayer is enhanced when N₂ is adsorbed. Meanwhile, the results also demonstrate the contribution of the *d* orbital of TM to the deformation of the whole DOS curve. The hybridization of the *p* and *d* orbitals of the N and the TM atoms ameliorates N₂ adsorption. Compared with Figure 7c, the Ni-InN monolayer achieves an electrical response only to N₂ (conductivity enhanced), when CO₂ and N₂ are co-adsorbed.

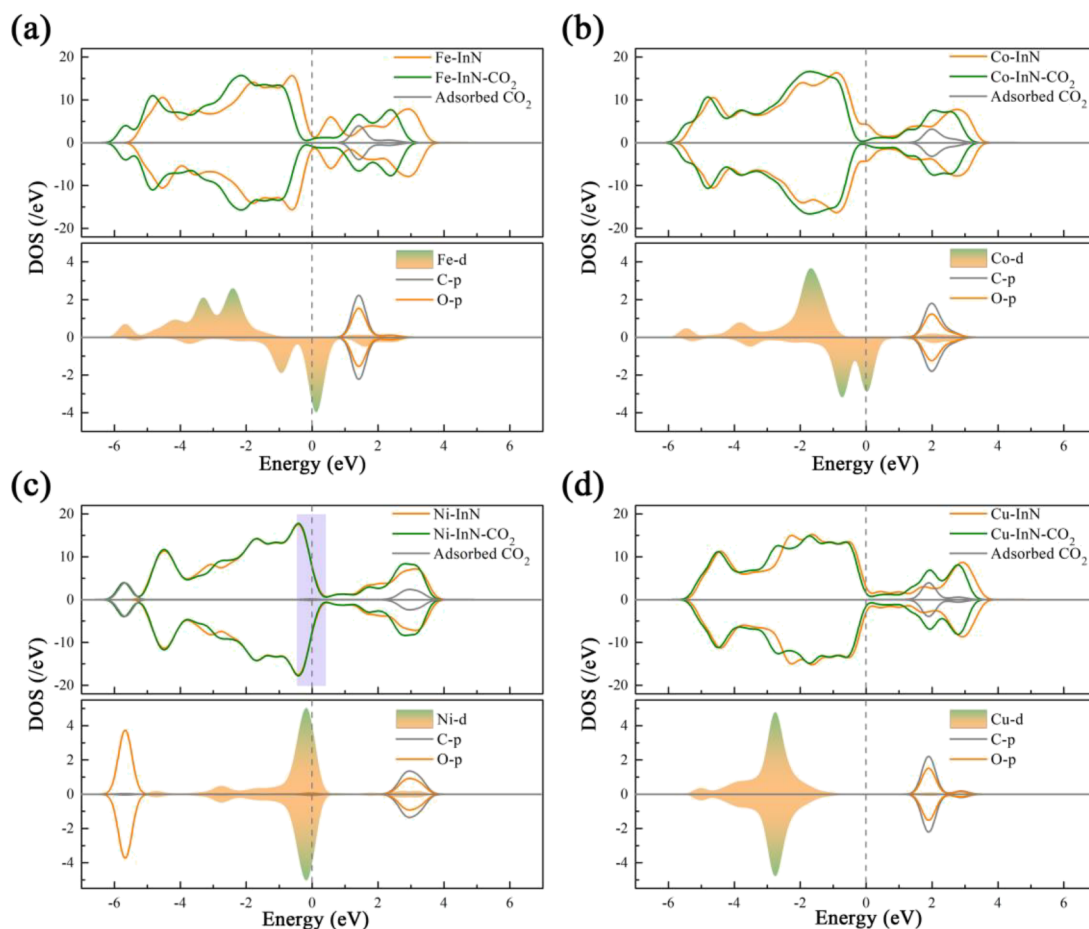


Figure 7. DOS of (a) Fe-InN-CO₂, (b) Co-InN-CO₂, (c) Ni-InN-CO₂, and (d) Cu-InN-CO₂.

It is easy to perform a quantitative analysis for a single gas based on our previous study.²⁸ Since the adsorption of CO₂ and N₂ causes a change in the conductivity of TM-InN, for the InN decorating of Fe, Co, and Cu atoms, the trends of change in conductivity are the same, whether CO₂ or N₂. It proves that there is no way to distinguish between the respective contributions of CO₂ or N₂. For the Ni-InN monolayer, the surface conductivity does not change after CO₂ adsorption, but it increases during N₂ adsorption. It strongly suggests that the Ni-InN monolayer can distinguish between the two gases by changes in electrical conductivity, thus achieving a unique response to N₂.

3.3.3. Mechanism of Gas Sensing. To reveal the underlying mechanism of the different adsorption behaviors induced by the TM atoms decorating, the d-band center of the TM-InN is calculated to describe the gas adsorption properties of the TM atoms. The hybridization of the *p* and *d* orbitals of the *N* and the TM atoms, respectively, promotes the binding of adsorbate and adsorbent,³⁸ which leads to the formation of the filled bonding and antibonding states. According to previous research,⁶⁸ the d-band center (ε_d) can be described as

$$\varepsilon_d = \frac{\int_{-\infty}^{\infty} n_d(\varepsilon)\varepsilon d\varepsilon}{\int_{-\infty}^{\infty} n_d(\varepsilon)d\varepsilon} \quad (4)$$

where ε is the energy and $n_d(\varepsilon)$ is the density. Figure 9a shows the projected DOS (PDOS) as well as ε_d of the TM-InN monolayer. Results illustrate that ε_d of TM-InN shifts toward higher energy, in an order of Ni-InN > Co-InN > Cu-InN >

Fe-InN. Notably, the order of ε_d coincides with the order of N₂ adsorption energy on the TM-InN (Figure 6a). In light of the d-band center theory, ε_d is positively correlated to metal-adsorbent interactions. As shown in Figure 9b, ε_d of Ni-InN is the closest to the Fermi level, proving that the proportion of unoccupied antibonding states is increased, leading to the strongest interaction between N₂ and Ni-InN. Similar results are suitable for the adsorption of CO₂ on the Ni-InN monolayer.

However, Figure 6a shows the opposite conclusions regarding the adsorption energy of CO₂ and N₂ on Cu-InN and Co-InN. Because N₂ exhibits strong chemisorption on the TM decorating surface, thus satisfying the law of the d-band center theory. Significantly, the adsorption of CO₂ on TM-InN is at the edge of physical and chemical adsorption, so it has a weak interaction. Meanwhile, it is found from the charge density distribution map that the charge transfer of CO₂ on Fe-InN and Co-InN is almost negligible, and that of Ni-InN and Cu-InN has significant electron overlap to form chemisorption. Hence, the adsorption energy of CO₂ only on Ni-InN and Cu-InN satisfies the law of ε_d as shown in Figure 9a. These results prove that ε_d of the TM site is one of the significant factors impacting the gas activation.

3.4. Applications of the N₂ Sensor. Different materials have their own optimal operating temperature intervals.^{69,70} As everyone knows, the DFT calculation is performed under the ideal condition of 0 K to obtain the feasibility of reaction. With rising of temperature, the thermodynamic advantage of gas adsorption will disappear. However, few studies have focused

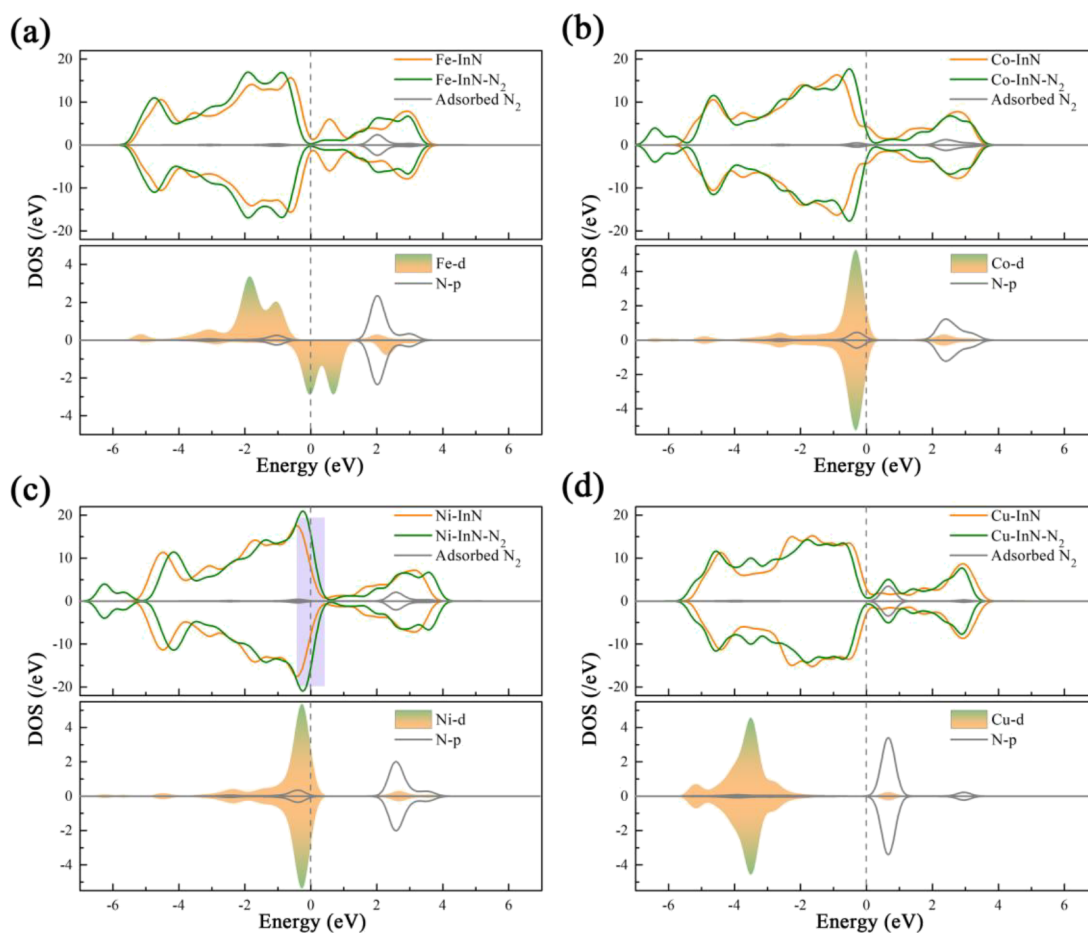


Figure 8. DOS of (a) Fe-InN-N₂, (b) Co-InN-N₂, (c) Ni-InN-N₂, and (d) Cu-InN-N₂.

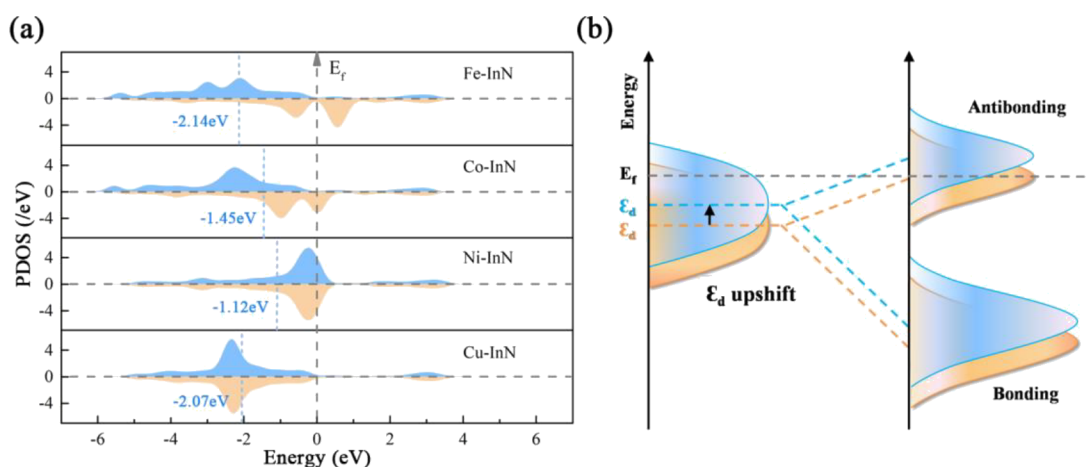


Figure 9. Illustration of the adsorption mechanism. (a) PDOS and d-band center of TM-InN and (b) metal–adsorbate interaction by altering the metal d-band center.

on the thermodynamic spontaneity of the adsorption behavior as a function of temperatures. Therefore, it is necessary to compute the thermodynamics of TM-InN sensitivity to CO₂ and N₂ at different temperatures to evaluate its application. Thermodynamic properties are calculated from 0 to 1000 K by the atomic vibration frequency. The details of thermodynamic calculation are provided in the [Supporting Information](#).

Changes in the Gibbs free energy (ΔG) (Figure 10) can be obtained based on the enthalpy changes (ΔH) and entropy

changes (ΔS) (Figures S11–S14). Figure 10 displays that ΔG of CO₂ and N₂ is linearly associated with temperatures. It can be found that the upper limit temperature for the thermodynamic spontaneity of CO₂ adsorption on the TM-InN is approximately 700 K (Ni-InN). However, N₂ on the TM-InN is approximately 950 K (Ni-InN). It demonstrates that the Ni-decorated InN monolayer significantly outperforms the other three TM atoms. Therefore, the Ni-InN monolayer

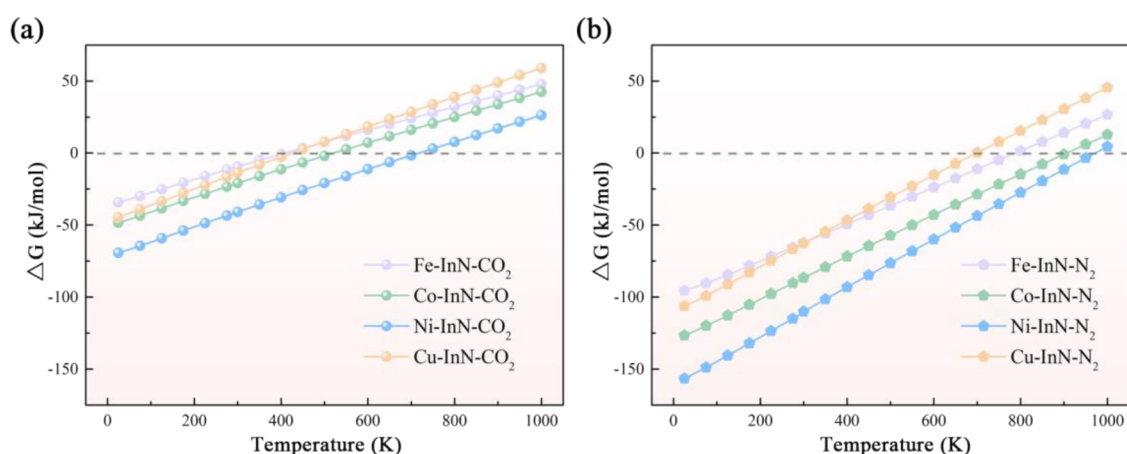


Figure 10. Thermodynamic property of (a) CO₂ and (b) N₂ adsorbed on the TM-InN monolayer as a function of temperatures.

senses N₂ in a wide temperature range due to high thermodynamic spontaneity.

4. CONCLUSIONS

In summary, DFT calculation with dispersion-corrections is performed to clarify the gas sensitive behavior of CO₂ and N₂ on the TM-InN monolayer. The findings of this research demonstrate that CO₂ and N₂ are physically adsorbed on the neat InN monolayer. After decorating TM atoms, binding and cohesive energy are compared to illustrate the surface stability. Based on DOS analysis, the Ni decorating InN monolayer can improve the conductivity more than the other three TM atoms. In addition, CO₂ and N₂ prefer the vertical adsorption configuration on the Ni-InN monolayer due to the obvious electronic overlap. The adsorption energy of N₂ on Ni-InN is dramatically enhanced from -0.1 to -1.93 eV, and that of CO₂ is from -0.2 to -0.66 eV. Charge transfer, bond length, and the Mayer bond order also prove that N₂ is significantly activated over CO₂, so the Ni-InN monolayer has a stronger affinity toward N₂. Noticeably, we clearly show for the first time that the Ni-InN monolayer achieves a single electrical response to N₂ according to DOS analysis, while removing the interference of CO₂. Additionally, the d-band center theory was utilized to understand the underlying mechanism of gas adsorption on the Ni-InN monolayer with ϵ_d upshift. Finally, we highlight the advantages of the Ni-InN monolayer in practical applications based on thermodynamic calculations from 0 to 950 K. Therefore, the Ni-InN monolayer can act as a potential highly selective N₂ sensor.

■ ASSOCIATED CONTENT

SI Supporting Information

The Supporting Information is available free of charge at <https://pubs.acs.org/doi/10.1021/acsami.2c21463>.

Adsorption properties of gas on the pristine InN monolayer, AIMD of the TM-InN monolayer, horizontal adsorption of gas on the TM-InN monolayer, binding energy of TM atoms to the InN monolayer, cohesive energy of the TM-InN monolayer, energy fluctuations with time process for the ab initio molecular dynamics of the TM-InN monolayer, horizontal adsorption configurations, COHP between gas and the TM-InN monolayer, ΔH and ΔS of CO₂ and N₂ adsorbed on

the TM-InN surface as a function of temperature, and details of thermodynamic calculations (PDF)

■ AUTHOR INFORMATION

Corresponding Authors

Lin Tao – School of Chemical Engineering, University of Science and Technology Liaoning, Anshan 114051, China; orcid.org/0000-0002-3268-7009; Email: taolin_phd@163.com

Davoud Dastan – Department of Materials Science and Engineering, Cornell University, Ithaca, New York 14850, United States; orcid.org/0000-0002-4124-5763; Email: d.dastan61@yahoo.com

Lixiang Li – School of Chemical Engineering, University of Science and Technology Liaoning, Anshan 114051, China; Email: lxli2005@126.com

Baigang An – School of Chemical Engineering, University of Science and Technology Liaoning, Anshan 114051, China; Email: baigang73@126.com

Authors

Wensen Wang – Institut Européen des Membranes, Université Montpellier, Montpellier 34000, France

Preeyaporn Poldorn – Center of Excellence in Biocatalyst and Sustainable Biotechnology, Department of Biochemistry, Faculty of Science, Chulalongkorn University, Bangkok 10330, Thailand

Xianze Meng – School of Materials, Sun Yat-sen University, Guangzhou 510006, China; orcid.org/0000-0002-3107-9570

Mingjie Wu – Department of Chemical Engineering, McGill University, Montreal, Quebec H3A 0C5, Canada

Hongwei Zhao – School of Chemical Engineering, University of Science and Technology Liaoning, Anshan 114051, China

Han Zhang – School of Chemical Engineering, University of Science and Technology Liaoning, Anshan 114051, China; orcid.org/0000-0001-6905-0952

Complete contact information is available at: <https://pubs.acs.org/doi/10.1021/acsami.2c21463>

Author Contributions

[†]L.T. and D.D. contributed equally.

Notes

The authors declare no competing financial interest.

ACKNOWLEDGMENTS

The funding from the National Natural Science Foundation of China (Grant Nos. 51972156, 51872131, and 22109061), the Youth Fund of the Education Department of Liaoning Province (LJKQZ20222324 and 2020LNQN17), and University of Science and Technology Liaoning Talent Project Grants (601010398) is gratefully acknowledged. We also thank Dr. Aleksandar Živković (Utrecht University, The Netherlands) for reading the manuscript.

REFERENCES

- (1) Zhang, M.; Shi, Z.; Zhang, J.; Zhang, K.; Lei, L.; Dastan, D.; Dong, B. Greatly Enhanced Dielectric Charge Storage Capabilities of Layered Polymer Composites Incorporated with Low Loading Fractions of Ultrathin Amorphous Iron Phosphate Nanosheets. *J. Mater. Chem. C* **2021**, *9*, 10414.
- (2) Han, M.; Shi, Z.; Zhang, W.; Zhang, K.; Wang, H.; Dastan, D.; Fan, R. Significantly Enhanced High Permittivity and Negative Permittivity in Ag/Al₂O₃/3D-BaTiO₃/epoxy Metacomposites with Unique Hierarchical Heterogeneous Microstructures. *Composites, Part A* **2021**, *149*, No. 106559.
- (3) Pecz, B.; Nicotra, G.; Giannazzo, F.; Yakimova, R.; Koos, A.; Kakanakova-Georgieva, A. Indium Nitride at the 2d Limit. *Adv. Mater.* **2021**, *33*, No. 2006660.
- (4) Fathinezhad, M.; AbbasiTarighat, M.; Dastan, D. Chemometrics Heavy Metal Content Clusters using Electrochemical Data of Modified Carbon Paste Electrode. *Environ. Nanotechnol., Monit. Manage.* **2020**, *14*, No. 100307.
- (5) Shan, K.; Yi, Z.; Yin, X.; Dastan, D.; Altaf, F.; Garmestani, H.; Alamgir, F. Mixed Conductivity Evaluation and Sensing Characteristics of Limiting Current Oxygen Sensors. *Surf. Interfaces* **2020**, *21*, No. 100762.
- (6) Haghnegahdar, N.; AbbasiTarighat, M.; Dastan, D. Curcumin-functionalized Nanocomposite AgNPs/SDS/MWCNTs for Electrocatalytic Simultaneous Determination of Dopamine, Uric Acid, and Guanine in Co-existence of Ascorbic Acid by Glassy Carbon Electrode. *J. Mater. Sci.: Mater. Electron.* **2021**, *32*, 5602–5613.
- (7) Anichini, C.; Czepa, W.; Pakulski, D.; Aliprandi, A.; Ciesielski, A.; Samori, P. Chemical Sensing with 2d Materials. *Chem. Soc. Rev.* **2018**, *47*, 4860–4908.
- (8) Poldorn, P.; Wongnongwa, Y.; Zhang, R.-Q.; Nutanong, S.; Tao, L.; Rungrotmongkol, T.; Jungsuttiwong, S. Mechanistic Insights into Hydrogen Production from Formic Acid Catalyzed by Pd@N-Doped Graphene: The Role of the Nitrogen Dopant. *Int. J. Hydrogen Energy* **2023**, DOI: 10.1016/j.ijhydene.2023.01.019.
- (9) Ashraf, I.; Ahmad, S.; Nazir, F.; Dastan, D.; Shi, Z.; Garmestani, H.; Iqbal, M. Hydrothermal Synthesis and Water Splitting Application of d-Ti₃C₂ MXene/V₂O₅ Hybrid Nanostructures as an Efficient Bifunctional Catalyst. *Int. J. Hydrogen Energy* **2022**, *47*, 27383–27396.
- (10) Ma, B.; Zhao, H.; Li, T.; Liu, Q.; Luo, Y.; Li, C.; Lu, S.; Asiri, A. M.; Ma, D.; Sun, X. Iron-Group Electrocatalysts for Ambient Nitrogen Reduction Reaction in Aqueous Media. *Nano Res.* **2021**, *14* (3), 555–569.
- (11) Zheng, J.; Sun, C.; Wang, Z.; Liu, S.; An, B.; Sun, Z.; Li, F. Double Ionic-Electronic Transfer Interface Layers for All-Solid-State Lithium Batteries. *Angew. Chem., Int. Ed.* **2021**, *60* (34), 18448–18453.
- (12) Dastan, D.; Shan, K.; Jafari, A.; Gity, F.; Yin, X.-T.; Shi, Z.; Alharbi, N. D.; Reshi, B. A.; Fu, W.; Talu, S.; Aljerf, L.; Garmestani, H.; Ansari, L. Influence of Nitrogen Concentration on Electrical, Mechanical, and Structural Properties of Tantalum Nitride Thin Films Prepared via DC Magnetron Sputtering. *Appl. Phys. A: Mater. Sci. Process.* **2022**, *128*, 400.
- (13) Novoselov, K. S.; Geim, A. K.; Morozov, S. V.; Jiang, D.; Katsnelson, M. I.; Grigorieva, I. V.; Dubonos, S. V.; Firsov, A. A. Two-Dimensional Gas of Massless Dirac Fermions in Graphene. *Nature* **2005**, *438*, 197–200.
- (14) Wang, Z.; Wang, G.; Liu, X.; Wang, S.; Wang, T.; Zhang, S.; Yu, J.; Zhao, G.; Zhang, L. Two-Dimensional Wide Band-Gap Nitride Semiconductor GaN and AlN Materials: Properties, Fabrication and Applications. *J. Mater. Chem. C* **2021**, *9*, 17201–17232.
- (15) Jovic, V.; Moser, S.; Ulstrup, S.; Goodacre, D.; Dimakis, E.; Koch, R.; Katsoukis, G.; Moreschini, L.; Mo, S. K.; Jozwiak, C.; et al. How Indium Nitride Senses Water. *Nano Lett.* **2017**, *17*, 7339–7344.
- (16) Sun, Q.; Li, Z.; Searles, D. J.; Chen, Y.; Lu, G.; Du, A. Charge-Controlled Switchable CO₂ Capture on Boron Nitride Nanomaterials. *J. Am. Chem. Soc.* **2013**, *135*, 8246–8253.
- (17) Guo, H.; Zhang, W.; Lu, N.; Zhuo, Z.; Zeng, X. C.; Wu, X.; Yang, J. CO₂ Capture on h-BN Sheet with High Selectivity Controlled by External Electric Field. *J. Phys. Chem. C* **2015**, *119*, 6912–6917.
- (18) Sheng, Z.-H.; Shao, L.; Chen, J.-J.; Bao, W.-J.; Wang, F.-B.; Xia, X.-H. Catalyst-Free Synthesis of Nitrogen-Doped Graphene Via Thermal Annealing Graphite Oxide with Melamine and Its Excellent Electrocatalysis. *ACS Nano* **2011**, *5* (6), 4350–4358.
- (19) Yin, X.; Zhou, W.; Dastan, D.; Li, J.; Tan, X.; Liu, Y.; Gao, X.; Ma, X. Selectivity Sensing Response of ZnO-xCo₃O₄ based Sensor to CO against CH₄. *Mater. Sci. Semicond. Process.* **2022**, *149*, No. 106883.
- (20) Zhou, W.; Dastan, D.; Yin, X.; Nie, S.; Wu, S.; Wang, Q.; Li, J. Optimization of Gas Sensing Properties of n-SnO₂/pxCuO Sensors for Homogenous Gases and the Sensing Mechanism. *J. Mater. Sci.: Mater. Electron.* **2020**, *31*, 18412–18426.
- (21) Yin, X.-T.; Wu, S.-S.; Dastan, D.; Nie, S.; Liu, Y.; Li, Z.-G.; Zhou, Y.-W.; Li, J.; Faik, A.; Shan, K.; Shi, Z.; Tarighat, M. A.; Ma, X.-G. Sensing Selectivity of SnO₂-Mn₃O₄ Nanocomposite Sensors for the Detection of H₂ and CO Gases. *Surf. Interfaces* **2021**, *25*, No. 101190.
- (22) Mortazavi, B.; Javvaji, B.; Shojaei, F.; Rabczuk, T.; Shapeev, A. V.; Zhuang, X. Exceptional Piezoelectricity, High Thermal Conductivity and Stiffness and Promising Photocatalysis in Two-Dimensional Mosi2n4 Family Confirmed by First-Principles. *Nano Energy* **2021**, *82*, No. 105716.
- (23) Mortazavi, B.; Silani, M.; Podryabinkin, E. V.; Rabczuk, T.; Zhuang, X.; Shapeev, A. V. First-Principles Multiscale Modeling of Mechanical Properties in Graphene/Borophene Heterostructures Empowered by Machine-Learning Interatomic Potentials. *Adv. Mater.* **2021**, *33*, No. 2102807.
- (24) Jiao, Y.; Du, A.; Zhu, Z.; Rudolph, V.; Smith, S. C. Adsorption of Carbon Dioxide and Nitrogen on Single-Layer Aluminum Nitride Nanostructures Studied by Density Functional Theory. *J. Phys. Chem. C* **2010**, *114*, 7846–7849.
- (25) Lee, S. H.; Kim, N.; Ha, D. G.; Kim, S. K. “Associative” Electron Attachment to Azabenzene-(CO₂)N Van Der Waals Complexes: Stepwise Formation of Covalent Bonds with Additive Electron Affinities. *J. Am. Chem. Soc.* **2008**, *130*, 16241–16244.
- (26) Yadav, V. K.; Mir, S. H.; Singh, J. K. Electronic Properties and Superior CO₂ Capture Selectivity of Metal Nitride (Xn) and Phosphide (Xp) (X = Al, Ga and In) Sheets. *Appl. Surf. Sci.* **2020**, *527*, No. 146445.
- (27) Tan, X.; Tahini, H. A.; Smith, S. C. Computational Design of Two-Dimensional Nanomaterials for Charge Modulated CO₂/H₂ Capture and/or Storage. *Energy Storage Mater.* **2017**, *8*, 169–183.
- (28) Yin, X.-T.; Tao, L. Fabrication and Gas Sensing Properties of Au-Loaded SnO₂ Composite Nanoparticles for Low Concentration Hydrogen. *J. Alloys Compd.* **2017**, *727*, 254–259.
- (29) Yin, X. T.; Li, J.; Wang, Q.; Dastan, D.; Shi, Z. C.; Alharbi, N.; Garmestani, H.; Tan, X. M.; Liu, Y.; Ma, X. G. Opposite Sensing Response of Heterojunction Gas Sensors Based on SnO₂-Cr₂O₃ Nanocomposites to H₂ against CO and Its Selectivity Mechanism. *Langmuir* **2021**, *37*, 13548–13558.
- (30) He, Y.; Li, J.; Tao, L.; Nie, S.; Fang, T.; Yin, X.; Wang, Q. First-Principles Calculations on the Resistance and Electronic Properties of H₂ Adsorption on a CoO-SnO₂ Heterojunction Surface. *Phys. Chem. Chem. Phys.* **2021**, *24*, 392–402.
- (31) Zhang, A.; Liang, Y.; Li, H.; Zhang, B.; Liu, Z.; Chang, Q.; Zhang, H.; Zhu, C. F.; Geng, Z.; Zhu, W.; et al. In-Situ Surface Reconstruction of Inn Nanosheets for Efficient CO₂ Electroreduction into Formate. *Nano Lett.* **2020**, *20*, 8229–8235.

- (32) Cui, H.; Jiang, J.; Gao, C.; Dai, F.; An, J.; Wen, Z.; Liu, Y. DFT Study of Cu-Modified and Cu-Embedded WSe₂ Monolayers for Cohesive Adsorption of NO₂, SO₂, CO₂, and H₂s. *Appl. Surf. Sci.* **2022**, *583*, No. 152522.
- (33) Thomas, S.; Asle Zaeem, M. Superior Sensing Performance of Two-Dimensional Ruthenium Carbide (2D-RuC) in Detection of NO, NO₂ and NH₃ Gas Molecules. *Appl. Surf. Sci.* **2021**, *563*, No. 150232.
- (34) Wu, M.; Zhang, G.; Wang, W.; Yang, H.; Rawach, D.; Chen, M.; Sun, S. Electronic Metal-Support Interaction Modulation of Single-Atom Electrocatalysts for Rechargeable Zinc-Air Batteries. *Small Methods* **2022**, *6*, No. 2100947.
- (35) Jayakrishnan, A.; Silva, J.; Kamakshi, K.; Dastan, D.; Annapureddy, V.; Pereira, M.; Sekhar, K. Are Lead-free Relaxor Ferroelectric Materials the Most Promising Candidates for Energy Storage Capacitors? *Prog. Mater. Sci.* **2023**, *132*, No. 101046.
- (36) Ju, L.; Tan, X.; Mao, X.; Gu, Y.; Smith, S.; Du, A.; Chen, Z.; Chen, C.; Kou, L. Controllable CO₂ Electrocatalytic Reduction Via Ferroelectric Switching on Single Atom Anchored In₂Se₃ Monolayer. *Nat. Commun.* **2021**, *12*, 5128.
- (37) Hu, L.; Du, Y.; Gao, L.; Di, M.; Zhang, N.; Pan, Y.; Yan, X.; An, B.; He, G. Nanoscale Solid Supercid-Coupled Polybenzimidazole Membrane with High Ion Selectivity for Flow Batteries. *ACS Sustainable Chem. Eng.* **2020**, *8* (44), 16493–16502.
- (38) Chen, J. W.; Zhang, Z.; Yan, H. M.; Xia, G. J.; Cao, H.; Wang, Y. G. Pseudo-Adsorption and Long-Range Redox Coupling During Oxygen Reduction Reaction on Single Atom Electrocatalyst. *Nat. Commun.* **2022**, *13*, 1734.
- (39) Wang, Z.; Qi, F.; Yin, L.; Shi, Y.; Sun, C.; An, B.; Cheng, H.-M.; Li, F. An Anion-Tuned Solid Electrolyte Interphase with Fast Ion Transfer Kinetics for Stable Lithium Anodes. *Adv. Energy Mater.* **2020**, *10* (14), 1903843.
- (40) Sun, C.; Wang, Z.; Yin, L.; Xu, S.; Ghazi, Z. A.; Shi, Y.; An, B.; Sun, Z.; Cheng, H.-M.; Li, F. Fast Lithium Ion Transport in Solid Polymer Electrolytes from Polysulfide-Bridged Copolymers. *Nano Energy* **2020**, *75*, 104976.
- (41) Li, S.; Zhang, H.; Wu, L.; Zhao, H.; Li, L.; Sun, C.; An, B. Vacancy-Engineered CeO₂/Co Heterostructure Anchored on the Nitrogen-Doped Porous Carbon Nanosheet Arrays Vertically Grown on Carbon Cloth as an Integrated Cathode for the Oxygen Reduction Reaction of Rechargeable Zn-Air Battery. *J. Mater. Chem. A* **2022**, *10* (18), 9858–9868.
- (42) Guo, Y.; Zhang, Y.; Wu, W.; Liu, Y.; Zhou, Z. Transition Metal (Pd, Pt, Ag, Au) Decorated Inn Monolayer and Their Adsorption Properties Towards NO₂: Density Functional Theory Study. *Appl. Surf. Sci.* **2018**, *455*, 106–114.
- (43) Cui, H.; Zhang, X.; Li, Y.; Chen, D.; Zhang, Y. First-Principles Insight into Ni-Doped Inn Monolayer as a Noxious Gases Scavenger. *Appl. Surf. Sci.* **2019**, *494*, 859–866.
- (44) Chen, D.; Zhang, X.; Tang, J.; Cui, Z.; Cui, H. Pristine and Cu Decorated Hexagonal Inn Monolayer, a Promising Candidate to Detect and Scavenge SF₆ Decompositions Based on First-Principle Study. *J. Hazard. Mater.* **2019**, *363*, 346–357.
- (45) Wang, Y.; Meng, Y.; Ni, Z.; Xia, S. Promotion of H₂ Adsorption Performance on Inn Monolayer by Embedding Cu Atom: A First-Principles Study. *Int. J. Hydrogen Energy* **2021**, *46*, 865–874.
- (46) Wang, H.; Wu, H.; Cui, H. Adsorption of H₂ and C₂H₂ onto Rh-Decorated InN Monolayer and the Effect of Applied Electric Field. *Mol. Phys.* **2022**, *120*, No. e2027535.
- (47) Zhu, P.; Dastan, D.; Liu, L.; Wu, L.; Shi, Z.; Chu, Q.; Altaf, F.; Mohammed, M. Surface Wettability of Various Phases of Titania Thin Films: Atomic-scale Simulation Studies. *J. Mol. Graphics Modell.* **2023**, *118*, No. 108335.
- (48) Timoumi, A.; Dastan, D.; Jamoussi, B.; Essalah, K.; Alsalmi, O.; Bouguila, N.; Abassi, H.; Chakroun, R.; Shi, Z.; Tãlu, Ș. Experimental and Theoretical Studies on Optical Properties of Tetra(Imidazole) of Palladium (II) Phthalocyanine. *Molecules* **2022**, *27*, 6151.
- (49) Wang, D.; Xu, H.; Yang, P.; Lu, X.; Ma, J.; Li, R.; Xiao, L.; Zhang, J.; An, M. Fe–N₄ and Co–N₄ Dual Sites for Boosting Oxygen Electroreduction in Zn–Air Batteries. *J. Mater. Chem. A* **2021**, *9*, 13678–13687.
- (50) Amiin, I. S.; Liu, X.; Pu, Z.; Li, W.; Li, Q.; Zhang, J.; Tang, H.; Zhang, H.; Mu, S. From 3d Zif Nanocrystals to Co-Nx/C Nanorod Array Electrocatalysts for Orr, Oer, and Zn-Air Batteries. *Adv. Funct. Mater.* **2018**, *28*, No. 1704638.
- (51) Tao, L.; Huang, J.; Dastan, D.; Li, J.; Yin, X.; Wang, Q. Flue Gas Separation at Organic-Inorganic Interface under Geological Conditions. *Surf. Interfaces* **2021**, *27*, No. 101462.
- (52) Tao, L.; Huang, J.; Dastan, D.; Wang, T.; Li, J.; Yin, X.; Wang, Q. New Insight into Adsorption Characteristics of CO₂ on the Surface of Calcite, Dolomite, and Magnesite. *Appl. Surf. Sci.* **2021**, *540*, No. 148320.
- (53) Tao, L.; Huang, J.; Dastan, D.; Wang, T.; Li, J.; Yin, X.; Wang, Q. CO₂ Capture and Separation on Charge-Modulated Calcite. *Appl. Surf. Sci.* **2020**, *530*, No. 147265.
- (54) Tao, L.; Huang, J.; Yin, X.; Wang, Q.; Li, Z.; Wang, G.; Cui, B. Adsorption Kinetics of CO₂ on a Reconstructed Calcite Surface: An Experiment-Simulation Collaborative Method. *Energy Fuels* **2019**, *33*, 8946–8953.
- (55) Poldorn, P.; Wongnongwa, Y.; Mudchimo, T.; Jungstittiwong, S. Theoretical Insights into Catalytic CO₂ Hydrogenation over Single-Atom (Fe or Ni) Incorporated Nitrogen-Doped Graphene. *J. CO₂ Util.* **2021**, *48*, No. 101532.
- (56) Potoff, J. J.; Siepmann, J. I. Vapor–Liquid Equilibria of Mixtures Containing Alkanes, Carbon Dioxide, and Nitrogen. *AIChE J.* **2001**, *47*, 1676–1682.
- (57) Zhang, L.; Hu, Z.; Jiang, J. Metal–Organic Framework/Polymer Mixed-Matrix Membranes for H₂/CO₂ Separation: A Fully Atomistic Simulation Study. *J. Phys. Chem. C* **2012**, *116*, 19268–19277.
- (58) Zhuo, S.; Huang, Y.; Hu, J.; Liu, H.; Hu, Y.; Jiang, J. Computer Simulation for Adsorption of CO₂, N₂ and Flue Gas in a Mimetic MCM-41. *J. Phys. Chem. C* **2008**, *112*, 11295–11300.
- (59) Kim, K.; Han, J. W.; Lee, K. S.; Lee, W. B. Promoting Alkali and Alkaline-Earth Metals on Mgo for Enhancing CO₂ Capture by First-Principles Calculations. *Phys. Chem. Chem. Phys.* **2014**, *16*, 24818–24823.
- (60) Ahmed, M. I.; Arachchige, L. J.; Su, Z.; Hibbert, D. B.; Sun, C.; Zhao, C. Nitrogenase-Inspired Atomically Dispersed Fe–S–C Linkages for Improved Electrochemical Reduction of Dinitrogen to Ammonia. *ACS Catal.* **2022**, *12*, 1443–1451.
- (61) Delley, B. From Molecules to Solids with the DMol³ Approach. *J. Chem. Phys.* **2000**, *113*, 7756–7764.
- (62) Perdew, J. P.; Wang, Y. Accurate and Simple Analytic Representation of the Electron-Gas Correlation Energy. *Phys. Rev. B: Condens. Matter* **1992**, *45*, 13244–13249.
- (63) Perdew, J. P.; Burke, K.; Ernzerhof, M. Generalized Gradient Approximation Made Simple. *Phys. Rev. Lett.* **1996**, *77*, 3865–3868.
- (64) Grimme, S. Semiempirical Gga-Type Density Functional Constructed with a Long-Range Dispersion Correction. *J. Comput. Chem.* **2006**, *27*, 1787–1799.
- (65) Mulliken, R. S. Electronic Population Analysis on Lcao–Mo Molecular Wave Functions. I. *J. Chem. Phys.* **1955**, *23*, 1833–1840.
- (66) Kumar, V.; Roy, D. R. Structure, Bonding, Stability, Electronic, Thermodynamic and Thermochemical Properties of Six Different Phases of Indium Nitride. *J. Mater. Sci.* **2018**, *53*, 8302–8313.
- (67) Zhang, X.; Wu, T.; Wang, H.; Zhao, R.; Chen, H.; Wang, T.; Wei, P.; Luo, Y.; Zhang, Y.; Sun, X. Boron Nanosheet: An Elemental Two-Dimensional (2d) Material for Ambient Electrocatalytic N₂-to-NH₃ Fixation in Neutral Media. *ACS Catal.* **2019**, *9*, 4609–4615.
- (68) Nørskov, J. K.; Studt, F.; Abild-Pedersen, F.; Bligaard, T. *Fundamental Concepts in Heterogeneous Catalysis*; John Wiley & Sons, Inc., 2014, Vol. 8; pp 114–137.
- (69) Dastan, D.; Shan, K.; Jafari, A.; Marszalek, T.; Mohammed, M. K. A.; Tao, L.; Shi, Z.; Chen, Y.; Yin, X.-T.; Alharbi, N. D.; et al. Influence of Heat Treatment on H₂s Gas Sensing Features of Nio Thin Films Deposited Via Thermal Evaporation Technique. *Mater. Sci. Semicond. Process.* **2023**, *154*, No. 107232.

(70) Wu, L.; Li, S.; Li, L.; Zhang, H.; Tao, L.; Geng, X.; Yang, H.; Zhou, W.; Sun, C.; Ju, D.; et al. Modest Modulation on the Electronic Structure of Co_9S_8 by Vanadium Doping for High-Performance Rechargeable Zn–Air Batteries. *Appl. Catal., B* **2023**, *324*, No. 122250.

Recommended by ACS

Ni Nanoclusters Anchored on Ni–N–C Sites for CO_2 Electroreduction at High Current Densities

Yanfang Song, Wei Wei, *et al.*

FEBRUARY 20, 2023

ACS APPLIED MATERIALS & INTERFACES

READ 

Ni-Doped Ti_3CNT_x -Coated Nanoporous Covalent Organic Frameworks to Accelerate Hydrogen Diffusion for Enhanced Hydrogen Evolution

Hui Zong, Ziqiang Zhu, *et al.*

OCTOBER 07, 2022

ACS APPLIED NANO MATERIALS

READ 

Modulating the Asymmetric Atomic Interface of Copper Single Atoms for Efficient CO_2 Electroreduction

Pengyu Song, Chen Chen, *et al.*

FEBRUARY 23, 2023

ACS NANO

READ 

Selective Formate Production from the Electrochemical CO_2 Reduction Reaction of Surface Oxide-Modified InSn_4 Binary Catalysts

Hsiao-Yun Liu, Kuan-Wen Wang, *et al.*

JULY 19, 2022

ACS APPLIED ENERGY MATERIALS

READ 

Get More Suggestions >